Rif1 Functions in a Tissue-Specific Manner To Control Replication Timing Through Its PP1-Binding Motif

Robin L. Armstrong,*,[1] Souradip Das,[†,1] Christina A. Hill,[‡] Robert J. Duronio,*,[‡,§,,††,2] and Jared T. Nordman[†,2]**

*Curriculum in Genetics and Molecular Biology, [‡]Integrative Program for Biological and Genome Sciences, [§]Department of Genetics, **Department of Biology, and [††]Lineberger Comprehensive Cancer Center, University of North Carolina, Chapel Hill, North Carolina 27599, and [†]Department of Biological Sciences, Vanderbilt University, Nashville, Tennessee 37232

ORCID IDs: 0000-0003-0018-4068 (R.L.A.); 0000-0002-8427-7749 (S.D.); 0000-0001-6469-6965 (R.J.D.); 0000-0002-6612-3201 (J.T.N.)

ABSTRACT Replication initiation in eukaryotic cells occurs asynchronously throughout S phase, yielding early- and late-replicating regions of the genome, a process known as replication timing (RT). RT changes during development to ensure accurate genome duplication and maintain genome stability. To understand the relative contributions that cell lineage, cell cycle, and replication initiation regulators have on RT, we utilized the powerful developmental systems available in *Drosophila melanogaster*. We generated and compared RT profiles from mitotic cells of different tissues and from mitotic and endocycling cells of the same tissue. Our results demonstrate that cell lineage has the largest effect on RT, whereas switching from a mitotic to an endoreplicative cell cycle has little to no effect on RT. Additionally, we demonstrate that the RT differences we observed in all cases are largely independent of transcriptional differences. We also employed a genetic approach in these same cell types to understand the relative contribution the eukaryotic RT control factor, Rif1, has on RT control. Our results demonstrate that Rif1 can function in a tissue-specific manner to control RT. Importantly, the Protein Phosphatase 1 (PP1) binding motif of Rif1 is essential for Rif1 to regulate RT. Together, our data support a model in which the RT program is primarily driven by cell lineage and is further refined by Rif1/PP1 to ultimately generate tissue-specific RT programs.

KEYWORDS DNA replication; *Drosophila*; endocycle; genome integrity; replication timing; Rif1

DNA replication begins at discrete initiation sites located within replication domains of the eukaryotic genome in a precise chronological manner during S phase. This temporal order of DNA replication is known as the DNA replication timing (RT) program. Although various mechanisms likely contribute to RT, RT programs are evolutionarily conserved from yeast to humans (Rivera-Mulia and Gilbert 2016). In metazoan species, replication domain sizes range from hundreds of kilobases to megabases, and their RT is correlated with transcriptional activity, chromatin structure, and position within the nucleus (MacAlpine *et al.* 2004; Schwaiger *et al.* 2009; Eaton *et al.* 2011; Rivera-Mulia and Gilbert 2016; Almeida *et al.* 2018). Furthermore, RT domains are highly correlated with topologically associated domains (TADs), where a near one-to-one correlation has been observed between RT domains and TADs (Pope *et al.* 2014). While RT is clearly influenced by chromatin structure and nuclear organization, the exact function of RT is not fully understood. Importantly, defects in RT are associated with genome instability, and RT is often altered in cancer cells (Stamatoyannopoulos *et al.* 2009; Koren *et al.* 2012; Donley and Thayer 2013). Therefore, understanding the processes and factors that contribute to RT is key to understanding fundamental aspects of eukaryotic DNA replication and genome stability.

Both cellular differentiation and cellular identity influence genome-wide RT, suggesting that the underlying mechanisms regulating RT are plastic during development. Comparison of

doi: https://doi.org/10.1534/genetics.120.303155
Manuscript received January 3, 2020; accepted for publication March 5, 2020; published Early Online March 6, 2020.
Available freely online through the author-supported open access option.

Supplemental material available at figshare: https://doi.org/10.25386/genetics.11920911.
[1]These authors contributed equally to this work.
[2]Corresponding authors: University of North Carolina, 3350 Genome Sciences Building, Chapel Hill, NC 27599. E-mail: duronio@med.unc.edu; Vanderbilt University, 465 21st Ave. S, Nashville, TN 37203. E-mail: jared.nordman@vanderbilt.edu

genome-wide RT between three lines of cultured *Drosophila* cells revealed differences in RT across ~8% of the genome (Lubelsky *et al.* 2014). More extensive RT profiling using *in vitro* models of cellular differentiation from multiple mammalian cell lineages has revealed ~50% of the genome is subject to cell-type-specific RT changes (Hiratani *et al.* 2008; Hiratani *et al.* 2010). Furthermore, in mammalian cells, the RT program goes through a global reorganization where many small RT domains consolidate into larger RT domains as cells differentiate from embryonic stem cells to more differentiated cell types (Ryba *et al.* 2010). It is still unclear, however, whether cell-type-specific changes in RT are developmentally programmed directly or whether differential RT is a passive reflection of the changes in chromatin structure and nuclear organization that occur during cellular differentiation.

Multiple *trans*-acting replication factors control RT from yeast to humans. Loading of the MCM replicative helicase during G1 phase of the cell division cycle and helicase activation during S phase are key steps in RT control (Bell and Stillman 1992; MacAlpine *et al.* 2010; Mantiero *et al.* 2011; Collart *et al.* 2013; Miotto *et al.* 2016). Several factors are limiting for replication initiation (Sld2, Sld3, Dpb11, Dbf4, and Cdc45) and their overexpression disrupts RT in budding yeast and *Xenopus* (Mantiero *et al.* 2011; Collart *et al.* 2013). A critical *trans*-acting RT-regulating factor is Rap1-interacting factor 1 (Rif1), which controls RT from yeasts to humans (Cornacchia *et al.* 2012; Hayano *et al.* 2012; Yamazaki *et al.* 2012; Peace *et al.* 2014; Foti *et al.* 2016). In animals, it is not clear whether the genomic regions that Rif1 targets during differentiation are cell-type-specific or whether Rif1 selectively regulates specific regions of the genome regardless of cell type. Although Rif1 is only modestly conserved, all Rif1 orthologs contain a Protein Phosphatase 1 (PP1)-interaction motif, suggesting that PP1 recruitment is a critical function of Rif1. Rif1-dependent recruitment of PP1 to chromatin may prevent the Dbf4-dependent kinase (DDK) activation of loaded helicases (Davé *et al.* 2014; Hiraga *et al.* 2014; Mattarocci *et al.* 2014; Hiraga *et al.* 2017; Sukackaite *et al.* 2017). However, how loss of the Rif1-PP1 interaction affects RT genome-wide has not been determined.

To better understand the extent to which Rif1 regulates RT in various unperturbed cell types during development, we have measured RT in the *Drosophila* larval wing discs and adult ovarian follicle cells in the presence and absence of Rif1. Here, we identify regions of the genome that change RT as a function of cell lineage and determine Rif1-dependent changes in RT in different tissue types. We found that cell lineage is a major driver of RT and demonstrate that tissue-specific transcription is not a major contributor to tissue-specific RT. Importantly, although RT in a subset of the genome depends on Rif1 similarly in different tissues, Rif1 acts in a tissue-specific manner to control RT. Additionally, the Rif1-PP1 interaction motif is required for Rif1-dependent control of RT, suggesting that PP1 recruitment to replicative helicases is the predominant mechanism Rif1 utilizes for RT control.

Materials and Methods

FACS and genomic DNA sequencing

Isolated nuclei from *OregonR*, *Rif1*^{1}/*Rif1*^{2} *(Rif1*$^{-}$*)*, and *Rif1*^{PP1}/*Rif1*^{1} *(Rif1*^{PP1}*)* female adult ovaries and *yw*, *Rif1*$^{-}$, and *Rif1*^{PP1} female third instar larval wing imaginal discs were sorted into G1 and S populations by a FACSAria II or III based on DAPI intensity and subsequently pelleted, flash-frozen, and stored at −80° before DNA isolation and library preparation. Libraries were prepared with the Rubicon ThruPLEX DNA-seq kit for wing imaginal disc samples and with the NEBNext Ultra II DNA Library Prep kit for follicle cell samples, and subjected to Illumina HiSeq 2500 single-end 50-bp sequencing for wing imaginal disc samples and Illumina HiSeq X or Novaseq 6000 paired-end 150-bp sequencing for follicle cell samples.

RT characterization

Reads from G1 and S samples were aligned to the dm6 reference genome (release 6.04) using Bowtie 2 (v2.3.2) default parameters (Langmead *et al.* 2009). Reads with a MAPQ score >10 were retained using SAMtools (v1.9) (Li *et al.* 2009). BEDTools coverage (v2.26.0) was used to quantify the number of reads mapping to each 100-kb window, with results normalized to read depth (Quinlan and Hall 2010). RT values were obtained by averaging the S/G1 ratio of reads per million value from each S phase replicate for a particular window size. Profiles were generated by plotting the RT value at each window *vs.* genomic location. Quantile normalization was performed for comparisons between samples through the preprocess Core R package to equalize the dynamic range of RT values (Bolstad 2016). The limma statistical package was used to identify 100-kb windows with significantly altered RT values [lmFit, *P* value adjusted for multiple testing ($P < 0.01$); absolute $\log_2$ fold change > 0.1] (Newville *et al.* 2014). BEDTools intersect (v2.26.0) was used to determine overlap of 100-kb windows with −f 0.5 and −u parameters (Quinlan and Hall 2010). RT values and limma-generated adjusted *P* values at 100-kb windows were used to determine median RT values and adjusted *P* values at 10-kb windows (BEDTools map v2.26.0), and the significance threshold was adjusted at 10-kb windows [*P* value adjusted for multiple testing ($P < 0.05$); absolute $\log_2$ fold change > 0.1] (Quinlan and Hall 2010). Coordinates of chromatin states were obtained from Kharchenko *et al.* (2011) and converted to dm6 coordinates using the UCSC liftOver tool (Karolchik *et al.* 2004). To calculate RT domain sizes, we identified the genomic coordinates halfway between each peak and valley of an RT profile and determined the distance from one halfway point to the next.

For false discovery rate calculations, spike-in RT bed files with 3×10^7 reads were generated by combining either 3×10^5 (1% impure), 1.5×10^6 (5% impure), 3×10^6 (10% impure), 7.5×10^6 (25% impure), or 1.5×10^7 (50% impure) randomly selected reads from each wing disc S phase replicate with 2.97×10^7 (1% impure), 2.85×10^7 (5%

impure), 2.7×10^7 (10% impure), 2.25×10^7 (25% impure), or 1.5×10^7 (50% impure) randomly selected reads from each mitotically cycling follicle cell S phase replicate. RT profiles generated from each test data set (1% impure, 5% impure, 10% impure, 25% impure, and 50% impure) were directly compared to RT profiles from wing discs, and differential RT was identified as before using the limma statistical package [lmFit, P value adjusted for multiple testing ($P < 0.01$); absolute $\log_2$ fold change > 0.1] (Newville *et al.* 2014). We estimate that 50% of the "mitotic" follicle cell population consists of endocycling follicle cells due to the following rationale: Because the total number of follicle cells in an egg chamber after the completion of the mitotic cell divisions is 1024, the 2C–4C population used for sorting contains 2^{10} (1024) mitotically cycling follicle cells from all egg chambers before stage 7 per ovariole and (at most) 1024 endocycling follicle cells from the stage 7 egg chamber per ovariole.

RNA analyses

Follicle cell isolation, RNA extraction and sequencing: Follicle cells were isolated by trypsinizing ovaries from *OregonR* or *Rif1*^{1}*/Rif1*^{2} females as described by Cayirlioglu *et al.* (2003) and Kim *et al.* (2011). Follicle cells were FACS-sorted into TRIzol LS (Invitrogen, Carlsbad, CA) based on their ploidy and RNA was extracted according to the manufacture's recommendation. A total of 250,000–500,000 follicle cells were used per replicate. Ribosomal RNA was depleted using the RiboMinus Eukaryote Kit for RNA-sequencing (Invitrogen) and libraries were prepared using the NEBNext Ultra II RNA Library Prep.

Wing disc isolation, RNA extraction and sequencing: Total RNA was isolated from 40 *yw* and *Rif1*^{1}*/Rif1*^{2} female third instar wing imaginal discs. Wing imaginal discs were homogenized in TRIzol (Invitrogen) and flash-frozen in liquid nitrogen. RNA was isolated using the Direct-zol RNA miniprep kit (Zymo Research). Ribosomal RNA was depleted and libraries were prepared using the Ovation *Drosophila* RNA-Seq system (NuGEN). RNA isolated from *yw* wing imaginal discs was also made into libraries and sequenced with follicle cell RNA for all comparisons in Figure 2.

RNA-sequencing analysis: TopHat default parameters (v2.1.1) (Trapnell *et al.* 2012) were used to align paired-end reads to the dm6 version of the *Drosophila* genome. Transcriptomes were generated using Cufflinks (v2.2.1). Differentially expressed transcripts were determined via edgeR statistical analysis (P value <0.01) (Robinson *et al.* 2010; McCarthy *et al.* 2012). For analyses comparing transcription to RT at 10-kb windows, we either assigned the average RNA $\log_2$ fold change and average adjusted P-value from all transcripts overlapping each 10-kb window or we assigned the $\log_2$ fold change of the transcript with the lowest edgeR-generated P value at each 10-kb window. Results were similar irrespective of how transcription was assigned to RT windows.

Data availability

The data generated as a part of this study have been submitted to the NCBI Gene Expression Omnibus under accession number GSE141632. All unique research materials and data will be freely available to other investigators. Supplemental material available at figshare: https://doi.org/10.25386/genetics.11920911.

Results

Cell lineage is a major driver of DNA RT

To analyze RT in unperturbed cell types and tissues without the need to immortalize or transform cells, we exploited the well-characterized developmental systems of *Drosophila melanogaster*. To determine how cell lineage affects RT, we generated genome-wide RT profiles from cells of two distinct *D. melanogaster* epithelial tissues: third instar larval wing imaginal disc cells and follicle cells from female adult ovaries. Cells of the wing disc are derived from the embryonic mesoderm, while ovarian follicle cells are derived from the embryonic ectoderm. To generate RT profiles, we used FACS to isolate and subsequently sequence the genomes of S phase nuclei from each tissue and compared these data to those obtained from G1 phase nuclei from wing discs, which serve as the copy number control for all samples (Figure 1A). We previously used this method to generate RT profiles in wild-type and mutant wing discs (Figure 1A; Armstrong *et al.* 2018). The premise of this method is that early-replicating DNA sequences are overrepresented relative to late-replicating sequences within the S phase population. Therefore, RT values can be quantified by determining $\log_2$-transformed S/G1 read counts across the genome, where larger values indicate earlier replication and smaller values indicate later replication (Figure 1A).

To determine how lineage contributes to RT, we generated RT values at 100-kb windows tiled at 10 kb intervals across the genome for both wing discs and follicle cells and used a stringent significance threshold to identify differential RT between each tissue (Materials and Methods; Armstrong *et al.* 2018). RT profiles generated from individual replicates of wild-type wing discs and follicle cells were strongly correlated (correlation coefficients = 0.95 and 0.95, respectively; *Materials and Methods*, Figure S1A, Figure S2), whereas RT values between the two lineages were significantly more divergent (correlation coefficient = 0.39; Figure 1B, Figure S14). A similar correlation was observed when 100-kb windows located in late-replicating pericentric heterochromatin were excluded from the analysis (correlation coefficient = 0.29; Figure S1B). While ~70% of the genome has similar RT between the two tissues, ~29% of the genome displays tissue-specific RT where 14.6% of windows replicate earlier in follicle cells and 14.5% of windows replicate earlier in wing discs (Figure 1, C and D, Figure S1C, Figure S14, and Table S1). Gene ontology analysis of genes located within tissue-specific RT domains did not reveal a significant

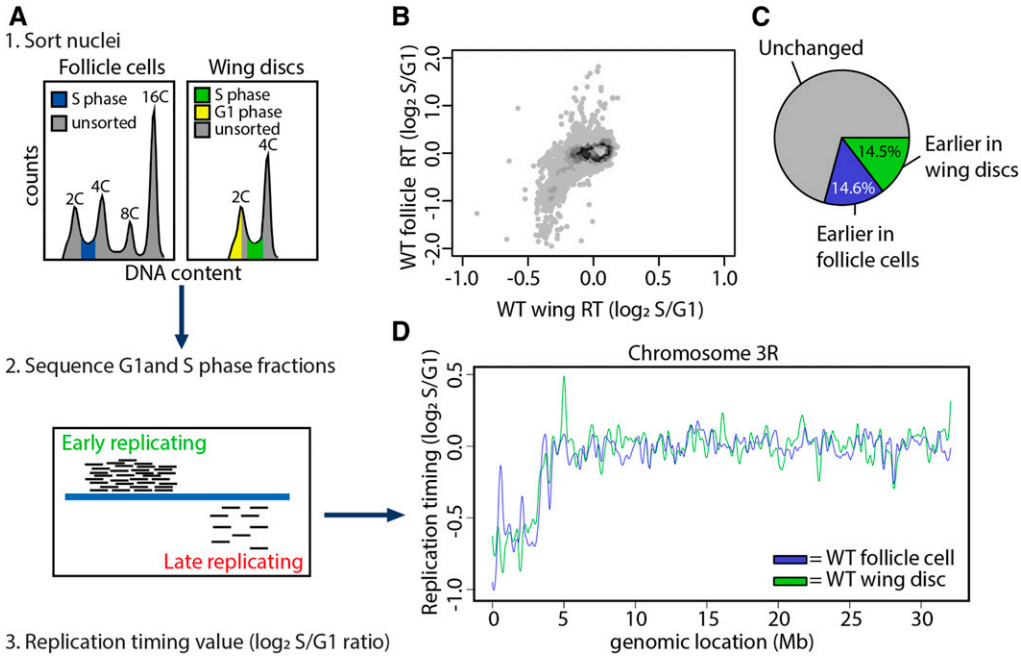

Figure 1 Cell lineage is a major driver of DNA replication timing in *Drosophila*. (A) Experimental outline: (1) Nuclei were FACS-sorted into G1 (yellow) and S (blue or green) populations based on DNA content. (2) DNA was sequenced and mapped back to the dm6 reference genome. The small black bars represent sequencing reads and the large blue bar represents the genome. More reads map to early than late-replicating sequences. (3) S/G1 $\log_2$ ratio of mapped reads generates replication timing profiles. (B) Heat scatter plot of wild-type wing disc and wild-type follicle cell S/G1 ($\log_2$) ratios at all 100-kb windows using a 10-kb slide across the genome. (C) Pie chart of all 100-kb windows of significantly earlier RT in wild-type wing discs (green), significantly earlier RT in wild-type follicle cells (blue), and unchanged RT (gray) across the major chromosome scaffolds. (D) LOESS regression lines showing average wild-type wing disc (green) and wild-type follicle cell (blue) S/G1 ($\log_2$) replication timing values across the chromosome 3R scaffold. See Figure S1 for all other chromosome arms. WT, wild type.

enrichment of genes associated with a specific biological process. Furthermore, differential RT between wing discs and follicle cells did not preferentially affect any one chromatin state (Kharchenko *et al.* 2011), and replication domain sizes were highly similar between the two tissues (Figure S1, D and E). These data demonstrate that cell lineage is a key contributor to RT control in *Drosophila*, similar to what has been previously observed in our previous analyses comparing wing disc and *Drosophila* cell lines (Lubelsky *et al.* 2014; Armstrong *et al.* 2018), and to analyses performed in mammalian cell culture systems (Hiratani *et al.* 2008; Ryba *et al.* 2010; Rivera-Mulia *et al.* 2015).

Cell-type-specific transcript levels do not drive changes in RT

Transcriptional activity is highly correlated with RT, with early-replicating regions of the genome associated with active transcription and late-replicating regions associated with transcriptional repression (MacAlpine *et al.* 2004; Liu *et al.* 2012; Lubelsky *et al.* 2014; Rivera-Mulia and Gilbert 2016). Therefore, we determined if differences in transcript abundance are correlated with differential RT. We generated transcriptomes from wild-type wing disc cells and follicle cells by total RNA-sequencing and identified differentially expressed transcripts between each tissue type. Individual biological replicates were highly correlated (Figure S3; correlation coefficients > 0.93) and we were able to identify tissue-specific transcripts including *wingless* (*wg*) in wing discs and *chorion protein* (*cp*) in follicle cells (Figure S4A). We observed 3994 differentially expressed transcripts ($P < 0.01$; edgeR) between the two tissues (Figure 2A), with elevated levels of 2651 transcripts in wing discs and 1343 transcripts in follicle cells (Figure 2A).

To identify whether tissue-specific RT is driven by tissue-specific transcription between wing discs and follicle cells, we directly compared differences in RT and transcript levels at 10-kb windows across the genome between the two tissues. First, we compared the average change in abundance of all transcripts within each window to the RT change of that window (*Materials and Methods*). Although transcript abundance was modestly elevated in wing discs *vs.* follicle cells at windows of earlier RT in wing discs [average $\log_2$ fold change = 1.45 counts per million (CPM)], we did not observe a strong correlation between elevated transcript abundance and earlier RT in follicle cells (Figure 2, B and C, Figure S4B). These results were consistent whether we considered (1) the average change in the abundance of all transcripts overlapping each 10-kb window (Figure 2, B and C, Figure S4B), (2) the change in abundance of the most confident transcript (lowest *P* value) assigned to each window (Figure S4C), (3) the change in abundance of the transcript with the greatest differential expression (absolute maximum $\log_2$ fold change) assigned to each window (Figure S4D), or (4) the RT change at all expressed genes (Figure S4E). Furthermore, 47.4% (791/1670) and 73.4% (813/1107) of windows with earlier RT in wing discs or follicle cells, respectively, do not contain a transcript with a significant increase in abundance (Figure S4F), suggesting that tissue-specific RT and tissue-specific transcription are mechanistically separable. Therefore, we conclude that differential transcript levels between wing discs and follicle cells does not fully explain differences in RT between these two tissues.

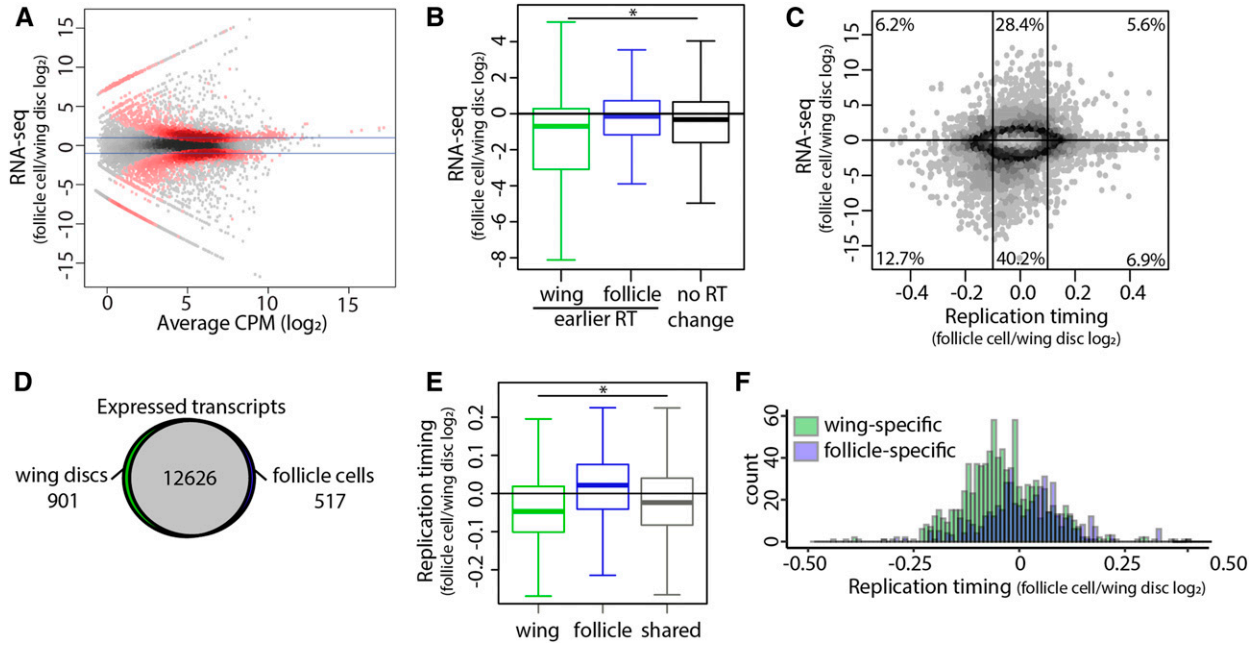

Figure 2 Tissue-specific transcription does not drive changes in RT. (A) Heat scatter plot of the wild-type follicle cell/wild-type wing disc ratio of total RNA-sequencing signal. Statistically different transcripts between wild-type follicle cells and wild-type wing discs are indicated in red ($P < 0.01$; edgeR). Blue lines indicate a $\log_2$ fold change of 1 and −1. (B) The average $\log_2$ fold change of all transcripts within each 10-kb window of earlier RT in wild-type wing discs (green), earlier RT in wild-type follicle cells (blue), and unchanged RT (black). Only windows containing at least one transcript are shown (* = $P < 0.0001$; one-way ANOVA). (C) Heat scatter plot of the wild-type follicle cell/wild-type wing disc RT values [S/G1 ($\log_2$)] *vs.* the wild-type follicle cell/wild-type wing disc ratio of normalized RNA-sequencing signal at all 10-kb windows across the major chromosome scaffolds. The average $\log_2$ fold change of all transcripts within each 10-kb window is plotted, and only windows containing at least one transcript are shown. Percentages represent the number of windows within each region (vertical lines at −0.1 and 0.1 represent $\log_2$ fold change cutoffs for RT statistical significance). (D) Venn diagram comparing expressed transcripts (transcripts per million (TPM) > 0) between wild-type wing discs and wild-type follicle cells. Wing-specific (green), follicle-specific (blue), and shared (gray) transcripts are indicated. (E) Log_2 fold change of RT values between wild-type follicle cells and wild-type wing discs at wing-specific (green), follicle-specific (blue), and shared (black) transcripts (* = $P < 0.0001$; one-way ANOVA). (F) Histogram of replication timing $\log_2$ fold change of wing-specific (green) and follicle-specific (blue) transcripts.

In our original assessment of transcription between tissue types, we noticed that the most extreme changes in transcript abundance tended to be expressed in a tissue-specific manner. Therefore, as an independent method to assess the relationship between tissue-specific transcript levels and RT, we identified transcripts present in both tissues (shared), transcripts present in wing discs only (wing-specific), and transcripts present in follicle cells only (follicle-specific) (*Materials and Methods*). We identified 12,626 genes that were expressed in both tissues, 901 genes that were wing-specific, and 517 that were follicle-specific (Figure 2D). When we quantified differential RT at both "shared" and tissue-specific genes, we observe earlier replication of wing-specific and "shared" genes in wing discs whereas follicle-specific genes do not replicate earlier in follicle cells (Figure 2, E and F). These data again indicate that tissue-specific transcript levels and tissue-specific RT, although correlated, are separable. We hypothesized that earlier replication of shared genes in wing discs would correlate with elevated transcript levels genome-wide in wing discs relative to follicle cells. Direct comparison of gene expression between the two tissues revealed a global increase of transcript abundance in wing discs relative to follicle cells (Figure S4, G and H). Together, these data demonstrate that while transcript levels and RT are correlated genome-wide (Figure S4, I and J), changes in transcript abundance do not direct changes in RT between wing discs and follicle cells, suggesting that RT and transcriptional activity are mechanistically separable.

The mitotic-to-endocycle transition does not affect DNA RT in follicle cells

The follicle cells of the adult ovary undergo a developmentally programmed cell cycle transition in which, after a series of mitotic divisions, they begin endocycling, a cell cycle consisting of S and G phases with no intervening mitoses (Figure 3A) (Edgar and Orr-Weaver 2001; Fox and Duronio 2013; Edgar *et al.* 2014). Follicle cells undergo three endocycles, resulting in a ploidy of 16C. Previous work has shown that there are distinct changes in genome regulation during the endocycle, including a global decrease in transcription, decrease in E2F1 target gene expression, and acquisition of endocycle-specific ORC binding sites (Maqbool *et al.* 2010; Sher *et al.* 2012; Hua *et al.* 2018; Rotelli *et al.* 2019). Therefore, we hypothesized that follicle cell RT may be influenced by this developmentally regulated cell cycle transition.

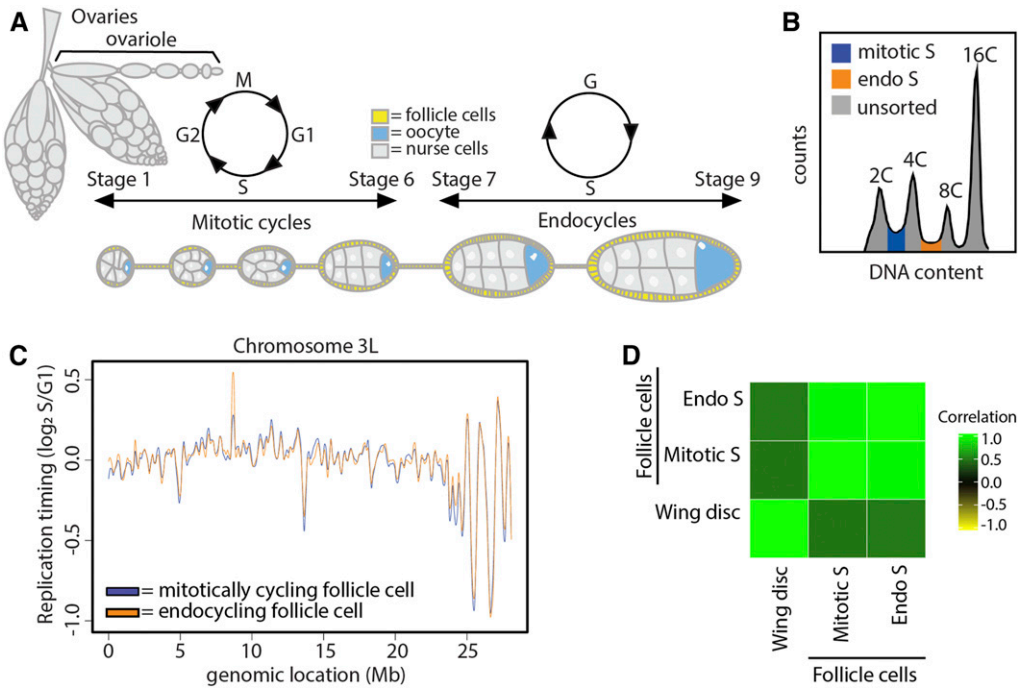

Figure 3 The mitotic-to-endocycle transition does not affect DNA replication timing within the follicle cells of the adult ovary. (A) Early egg chamber development within the adult *Drosophila* ovary. (B) Representative FACS profile of follicle cell nuclei isolated from whole ovaries. The 2C–4C S phase fraction (blue) are the mitotically cycling follicle cells, and the 4C–8C S phase fraction (orange) are the endocycling follicle cells. (C) LOESS regression line showing average wild-type mitotically cycling follicle cells (blue) and wild-type endocycling follicle cells (orange) S/G1 (log_2) replication timing values in at across the chromosome 3L scaffold. See Figure S5 for all other chromosome arms. (D) Correlation matrix of S/G1 (log_2) replication timing values for wild-type endocycling follicle cells (endo S), wild-type mitotically cycling follicle cells (mitotic S), and wild-type wing discs.

To determine if the transition from a mitotic cycle to an endocycle causes a change in RT, we generated genome-wide RT profiles from wild-type endocycling follicle cells and compared them to the RT profiles we measured from wild-type mitotic follicle cells (Figure S5, A and B). To this end, we collected the S phase populations between the 2C and 4C peaks (mitotic) and between the 4C and 8C peaks, which corresponds to the second of the three endocycles (Figure 3B). Direct comparison of RT profiles generated from wild-type mitotic (2C–4C) and endocycling (4C–8C) follicle cells showed no windows of differential RT genome-wide between the two populations of follicle cells (Figure 3, C and D, Figure S5C, Figure S14, and Table S1). Likewise, the gene expression profiles of these two populations of follicle cells were highly similar, with only six differentially expressed transcripts between mitotically cycling and endocycling follicle cells ($P < 0.01$, edgeR; Figure S3, Figure S5D). It is important to note that the first follicle cell endocycle likely initiates from G1 phase (Lilly and Spradling 1996; Calvi *et al.* 1998); therefore, the mitotic S phase sample may contain both mitotic and endocycling follicle cells. We were concerned that the impure cell population in the mitotic follicle cell data set might mask any differential RT between the mitotic and endocycling populations. Based on the number of follicle cells in a mature egg chamber (~1000), we estimate that follicle cells in the first endo S phase could account for, at most, half of the "mitotic" follicle cell population (2C–4C) (*Materials and Methods*). Therefore, we performed an *in silico* false discovery rate analysis by spiking in random reads from the wing disc RT data set into the mitotic follicle cell RT data set. Given that the endocycling follicle cells contribute no >50% of our total mitotic follicle cell population, we find that our analysis would be sensitive enough to accurately identify at least ~27% of the endocycle-specific RT differences (Figure S5E; *Materials and Methods*). Thus, endocycling S phase cells in the 2C–4C population do not mask a difference in RT between endocycling and mitotic follicle cells. Although we cannot exclude the possibility that minor changes in RT could be masked in our data, we conclude that mitotic and endocycling follicle cells have remarkably similar RT profiles, arguing that cell lineage, not changes in the cell cycle, is a major contributing factor to RT.

Rif1 fine tunes the RT program in different tissues

Rif1 is a global regulator of DNA RT from yeast to humans (Cornacchia *et al.* 2012; Hayano *et al.* 2012; Yamazaki *et al.* 2012; Peace *et al.* 2014; Seller and O'Farrell 2018). We sought to determine whether Rif1 regulates RT in a tissue-specific manner or whether Rif1-dependent RT domains are hardwired into the genome. To address these questions, we generated genome-wide RT profiles from mitotic follicle cells and wing discs in a *Rif1* null (*Rif1*$^-$) mutant previously generated by our laboratory (Figure S6, A and B; Munden *et al.* 2018). Individual replicates of *Rif1*$^-$ RT data generated from either wing discs or follicle cells correlated well (Figure S6C, Figure S7A, Figure S14), whereas comparison of *Rif1*$^-$ and wild-type RT data revealed that ~13% of the genome has differential RT in mitotically cycling follicle cells and 8% of the genome has differential RT in wing discs (correlation coefficients = 0.52 and 0.78, respectively; Figure S7B, Figure S6D, Figure S14). For the *Rif1*$^-$ mutant follicle cells, 8.2% of windows displayed advanced RT while 5.0% of windows had

delayed RT (Figure 4, A–C, Figure S7C, Figure S14, and Table S1). In the *Rif1*$^-$ mutant wing disc, 4.1% of windows had advanced RT and 3.9% of windows had delayed RT (Figure 4, A–C, Figure S6E, Figure S14, and Table S1). Furthermore, the magnitude of RT changes within windows of differential RT between *Rif1*$^-$ and wild type was significantly greater in follicle cells than that observed in wing discs (Figure 4, B and D). These data show that Rif1 has a greater effect on RT in follicle cells than wing discs, arguing that Rif1-dependent RT domains are not hardwired into the genome.

Rif1 promotes late replication likely by preventing replicative helicase activation (Hayano *et al.* 2012; Davé *et al.* 2014; Hiraga *et al.* 2014; Mattarocci *et al.* 2014; Hiraga *et al.* 2017). Therefore, we hypothesized that advanced RT in a *Rif1*$^-$ mutant is a direct effect of loss of Rif1 function, whereas delayed RT in a *Rif1*$^-$ mutant is a secondary effect. This hypothesis predicts that when comparing different *Rif1*$^-$ mutant cell types, there should be a greater extent of overlap between regions with advanced RT (direct) than between regions with delayed RT (indirect). We found that 43.8% (242/552) of windows with advanced RT in wing discs were also advanced in follicle cells. In contrast, only 16.9% (89/527) of windows with delayed RT in wing discs were also delayed in follicle cells (Figure 5A). These data support the hypothesis that advanced RT is a direct effect of Rif1 loss, whereas delayed RT is likely a secondary effect.

While measuring RT values for *Rif1*$^-$ mutant and control samples, we profiled *Rif1*$^{-/+}$ heterozygous follicle cells (Figure S8, A and B). To our surprise, this heterozygous genotype displayed an intermediate RT phenotype with 3.6% of windows with advanced RT and 1.6% of windows with delayed RT relative to wild-type follicle cells (Figure S8C; Table S1). Furthermore, 87.0% of windows with significantly advanced and 57.5% with significantly delayed RT in *Rif1*$^-$ heterozygotes were also affected in *Rif1*$^-$ follicle cells, indicating dependency on Rif1 function (Figure S8D). These data demonstrate that *Rif1* is haploinsufficient for RT control.

As an independent metric to address the specificity of commonly advanced and/or delayed RT changes, we asked whether common RT changes between mitotic follicle cells and wing discs were also detected in *Rif1*$^-$ endocycling follicle cells. We generated RT profiles from *Rif1*$^-$ endocycling follicle cells and found that individual replicates of RT data correlated well (Figure S9A). In contrast, 14.8% of windows displayed differential RT in *Rif1*$^-$ endocycling follicle cells relative to control with 7.2% being advanced and 7.6% being delayed (Figure 5B, Figure S9B, Figure S14, and Table S1). Although RT was similar between wild-type mitotic and endocycling follicles cells, a *Rif1* mutation affected these cell populations differently. We found that 72.1% (789/960) of advanced windows in *Rif1*$^-$ endocycling follicle cells were also advanced in *Rif1*$^-$ mitotic follicle cells, and only 37.9% (388/1024) of the windows that were delayed in *Rif1*$^-$ endocycling follicle cells were also delayed in *Rif1*$^-$ mitotic follicle cells (Figure S9C). Accordingly, the low degree of overlap between windows of delayed RT is reflected by the low genome-wide RT correlation between *Rif1*$^-$ mitotic and endocycling follicle cells (Figure 5B, Figure S9D, Figure S14). Interestingly, many of the regions of advanced RT changes that were in common between *Rif1*$^-$ wing discs and mitotic follicle cells were also detected in *Rif1*$^-$ endocycling follicle cells, while the delayed RT changes were mostly nonoverlapping [72.7% (176/242) and 47.2% (42/89), respectively]. Therefore, while Rif1 regulates RT in a tissue-specific manner, Rif1 appears to regulate RT in a core region of the genome regardless of cell type.

Rif1 controls RT of pericentric heterochromatin

Almost all commonly advanced windows in *Rif1*$^-$ mutant cell populations are located within pericentric heterochromatin, where Rif1 is known to localize by immunofluorescence (Buonomo *et al.* 2009; Munden *et al.* 2018; Seller and O'Farrell 2018). In contrast, all but eight of the commonly delayed windows are located along euchromatic chromosome arms (Figure 5C, Figure S10A). This relationship is also true for tissue-specific RT changes in *Rif1*$^-$ wing discs and follicle cells—advancements are overrepresented in pericentric heterochromatin whereas delays are overrepresented along chromosome arms (Figure S10B). Approximately 67% of follicle-cell-specific advancements and ~40% of wing-disc-specific advancements occur within pericentric heterochromatin. Collectively, these data suggest that Rif1 directly regulates late replication and may play a significant role in regulating late replication of pericentric heterochromatin. Interestingly, almost 40% of mappable pericentric heterochromatin advances in *Rif1*$^-$ follicle cells (both mitotically cycling and endocycling), whereas 2.8-fold fewer pericentric windows advance RT in *Rif1*$^-$ wing discs (Figure 5D, Figure S10B). Furthermore, the overall RT of *Rif1*$^-$ pericentric heterochromatin remains very late in wing discs relative to the average RT of the chromosome arms, and the magnitude of RT advancement is less than that observed in *Rif1*$^-$ pericentric heterochromatin in follicle cells (Figure 5E, Figure S6E). Therefore, Rif1 contributes more substantially to late replication of pericentric heterochromatin in follicle cells than in wing discs.

Some genomic regions of *Drosophila* endocycling cells are underreplicated relative to the rest of the genome; *i.e.*, they have reduced copy number relative to overall ploidy. This is particularly true in pericentric heterochromatin in salivary glands and follicle cells, and this underreplication requires Rif1 (Munden *et al.* 2018). Based on DNA content measurements by FACS, underreplication is thought to begin during the first follicle cell endocycle (Calvi and Spradling 1998). Consequently, because our RT protocol measures relative copy number in S phase *vs.* G1 phase, one possible explanation for the significantly earlier replication of pericentric heterochromatin in polyploid *Rif1*$^-$ follicle cells relative to diploid *Rif1*$^-$ wing discs is a loss of underreplication of pericentric heterochromatin. Multiple observations, however, indicate that we are measuring true changes in RT rather than the loss of underreplication in

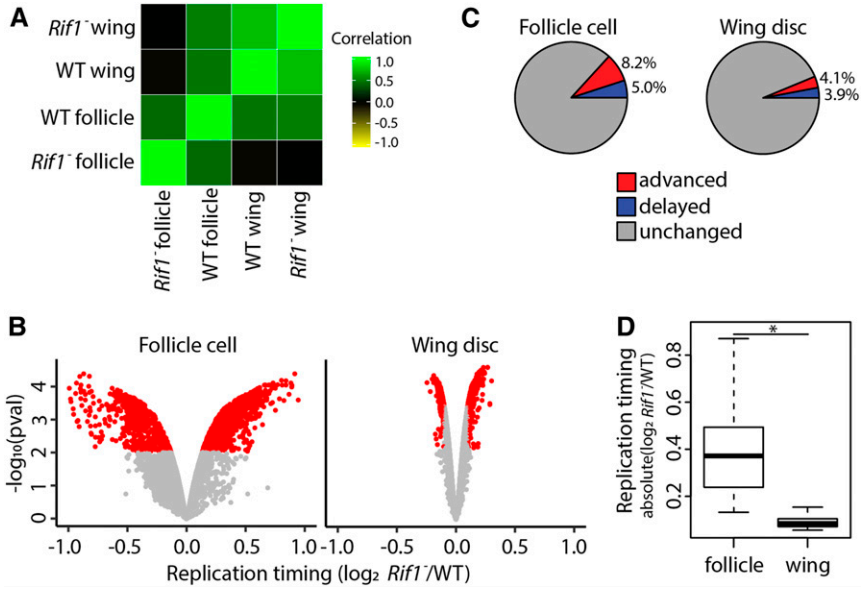

Figure 4 Rif1 regulates RT in a lineage-specific manner. (A) Correlation matrix of S/G1 ($\log_2$) replication timing values for wild-type mitotically cycling follicle cells (WT follicle), *Rif1*$^-$ mitotically cycling follicle cells (*Rif1*$^-$ follicle), wild-type wing discs (WT wing), and *Rif1*$^-$ wing discs (*Rif1*$^-$ wing). (B) Volcano plot of the *Rif1*$^-$/control ratio of normalized replication timing values [S/G1 ($\log_2$)] plotted *vs.* the $-\log_{10} P$ value (adjusted for multiple testing) in follicle cells (left) and wing discs (right). Significant replication timing changes are indicated (red; $P < 0.01$, absolute $\log_2$ fold change > 0.1; limma). (C) Pie chart of all 100-kb windows of significantly advanced RT (red), significantly delayed RT (blue), and unchanged RT (gray) across the major chromosome scaffolds in *Rif1*$^-$ mutants relative to wild-type control in follicle cells (left) and wing discs (right). (D) S/G1 ($\log_2$) absolute $\log_2$ fold change at 100-kb windows of significant RT change between *Rif1*$^-$ and control in follicle cells and wing discs (Student's *t*-test, * = $P < 2.2 \times 10^{-16}$).

Rif1$^-$ follicle cells. First, loss of underreplication predicts that nearly 100% of mappable pericentric heterochromatin would be scored as "advanced" RT. However, we found that only 40% of pericentric heterochromatin advances RT in *Rif1*$^-$ mitotic and endocycling follicle cells (Figure 5D, Figure S9B). Second, if pericentric heterochromatin was underreplicated in wild-type endocycling follicle cells, we would expect to observe a reduced copy number in pericentric heterochromatin relative to wild-type mitotically cycling follicle cells. However, pericentric heterochromatin copy number profiles derived from wild-type mitotic and endocycling S phase fractions are not different from one another (Figure S11). Together, these data support the conclusion that Rif1 regulates RT uniquely in different cell types and that the RT differences measured in *Rif1*$^-$ follicle cells represent changes in RT and do not result from changes in underreplication.

Rif1 controls RT independently of transcript levels

To determine whether RT changes in *Rif1*$^-$ wing discs and follicle cells were due to changes in transcript levels, we generated transcriptomes from *Rif1*$^-$ follicle cells and *Rif1*$^-$ wing discs. We identified only 121 and 60 differentially expressed transcripts between *Rif1*$^-$ and controls in wing discs and mitotic follicle cells, respectively, demonstrating that transcript abundance is largely unaffected after loss of Rif1 function (Figure S7D, Figure S3). We found only 2.1% (28/1342) of differential RT windows in follicle cells and 19.5% (99/507) of differential RT windows in wing discs contain at least one differentially expressed transcript (Figure 5F). Together, these data show that while loss of Rif1 function affects RT to a greater extent in follicle cells relative to wing discs, these RT changes likely do not result from changes in transcript levels.

Rif1's PP1 binding motif is essential for Rif1-mediated RT control

Rif1 affects the RT of pericentric heterochromatin to a greater extent in follicle cells than in wing discs (Figure 5, D and E), suggesting a different requirement for Rif1 in RT regulation of pericentric heterochromatin in different tissues. To further understand these mechanistic differences, we assessed what role the PP1 binding motif within Rif1 has on RT control of pericentric heterochromatin in wing discs and follicle cells. Rif1 orthologs from yeasts to humans contain a PP1 binding motif, and mutation of this motif prevents Rif1 association with PP1 in multiple systems (Davé *et al.* 2014; Hiraga *et al.* 2014; Mattarocci *et al.* 2014; Sreesankar *et al.* 2015; Alver *et al.* 2017; Hiraga *et al.* 2017; Sukackaite *et al.* 2017). We previously generated an allele of Rif1 (*Rif1*^{PP1}) where the conserved SILK/RSVF PP1 interaction motif is mutated to SAAK/RASA (Munden *et al.* 2018). We generated genome-wide RT profiles from *Rif1*^{PP1} wing discs and follicle cells. Individual replicates from each tissue correlated well (correlation coefficients = 0.91 and 0.89, respectively; Figure S12, A and B, Figure S13, A and B). In contrast, we found that 17.9% and 11% of windows in *Rif1*^{PP1} wing discs and follicle cells, respectively, displayed differential RT relative to control (Figure 6, A and B, Figure S12, C and D, Figure S13, C and D, Figure S14, and Table S1). Strikingly, *Rif1*^{PP1} wing discs displayed over threefold the number of advanced windows compared to *Rif1*$^-$ wing discs. In addition, almost all (94.4%) advanced windows in *Rif1*$^-$ wing discs were also advanced in *Rif1*^{PP1} mutants (Figure 6B). Interestingly, in follicle cells, there was almost a complete overlap of advanced RT windows between *Rif1*^{PP1} and *Rif1*$^-$ mutants. These data suggest that the *Rif1*^{PP1} and *Rif1*$^-$ mutations potentially affect RT through different mechanisms in wing discs and through the same mechanism in follicle cells. In contrast, the overlap

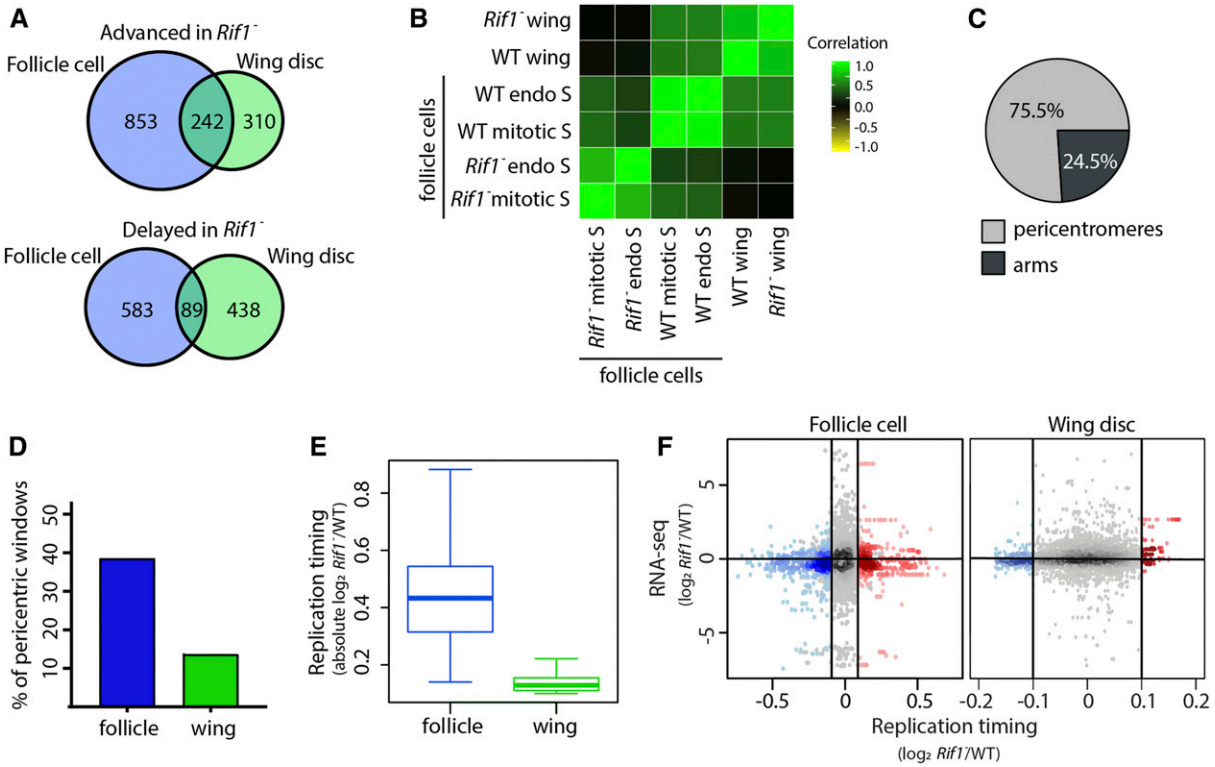

Figure 5 Rif1 promotes late replication of pericentric heterochromatin across lineages. (A) Venn diagrams comparing significantly advanced (top) and delayed (bottom) 100-kb windows identified in *Rif1*$^-$ follicle cells (left; blue) and wing discs (right; green) ($P < 0.01$ and absolute $\log_2$ fold change $>$ 0.1; limma). (B) Correlation matrix of S/G1 ($\log_2$) replication timing values for wild-type mitotically cycling follicle cells (WT mitotic S), *Rif1*$^-$ mitotically cycling follicle cells (*Rif1*$^-$ mitotic S), wild-type endocycling follicle cells (WT endo S), *Rif1*$^-$ mitotically cycling follicle cells (*Rif1*$^-$ endo S), wild-type wing discs (WT wing), and *Rif1*$^-$ wing discs (*Rif1*$^-$ wing). (C) Pie chart of all 100-kb windows of commonly advanced RT between *Rif1*$^-$ wing discs and follicle cells. Windows within pericentromeres are in gray and chromosome arms are in black. (D) Bar plot of the percentage of 100-kb windows in pericentric heterochromatin with significantly advanced RT. (E) S/G1 ($\log_2$) absolute $\log_2$ fold change at all 100-kb windows located in pericentric heterochromatin between *Rif1*$^-$ and control (Student's *t*-test, $P < 2.2 \times 10^{-16}$). (F) Heat scatter plot of the *Rif1*$^-$/control ratio of normalized replication timing values [S/G1 ($\log_2$)] plotted *vs.* the *Rif1*$^-$/control ratio of the most confident transcript (lowest *P* value) at each window across the major chromosome scaffolds. Significantly advanced (red) and delayed (blue) windows are indicated [$P < 0.05$, absolute $\log_2$ fold change $>$ 0.1 (vertical lines); limma].

of delayed RT changes between *Rif1*^{PP1} and *Rif1*$^-$ wing discs or follicle cells is poor (Figure 6B). These data further support that advanced RT in *Rif1* mutants is a direct consequence of Rif1 loss, whereas delayed RT is likely secondary effect.

As Rif1 affects RT of pericentric heterochromatin in both tissues, we hypothesized that RT changes in *Rif1*^{PP1} tissues would preferentially be located at pericentromeres. We found that ~48% of pericentric heterochromatin displayed a significant advancement of RT in *Rif1*^{PP1} wing discs, unlike what we found for *Rif1*$^-$ null wing discs, where only ~10% of pericentric heterochromatin advanced. The *Rif1*^{PP1} wing disc RT phenotype is more similar to what we observed at pericentric heterochromatin in *Rif1*$^-$ follicle cells (Figure 5A). Specifically, 80% (876/1095) of advanced windows in *Rif1*$^-$ mitotic follicle cells were also advanced in *Rif1*^{PP1} wing discs (Figure S13E). Additionally, all commonly advanced windows between *Rif1*$^-$ follicle cells and wing discs were advanced in *Rif1*^{PP1} wing discs. Interestingly, while the magnitude of RT change at pericentromeres is significantly greater in *Rif1*^{PP1} wing discs relative to *Rif1*$^-$ wing discs ($P < 2.2 \times 10^{-16}$), the magnitude of RT change in *Rif1*^{PP1} wing discs remains significantly lower than what is observed in *Rif1*$^-$ or *Rif1*^{PP1} follicle cells (Figure 6C). Collectively, these data demonstrate that the *Rif1*^{PP1} mutation differentially affects pericentric heterochromatin RT relative to the *Rif1*$^-$ mutation in wing discs and suggest that regulatory mechanisms, potentially including the Rif1-PP1 interaction, function differently to regulate late RT of pericentromeres between tissues.

Discussion

Our findings provide insight into the relative contributions that cell type, gene expression, cell cycle, and Rif1 have on RT control. By comparing genome-wide RT profiles from unperturbed cells from distinct tissues, we demonstrated that cell lineage has a larger effect on RT than Rif1, an evolutionarily conserved regulator of RT. We also found that the RT program is not modified in response to the physiological and transcriptional changes that occur during the mitotic-to-endocycle transition, and that transcriptional differences between cell types do not drive changes in RT.

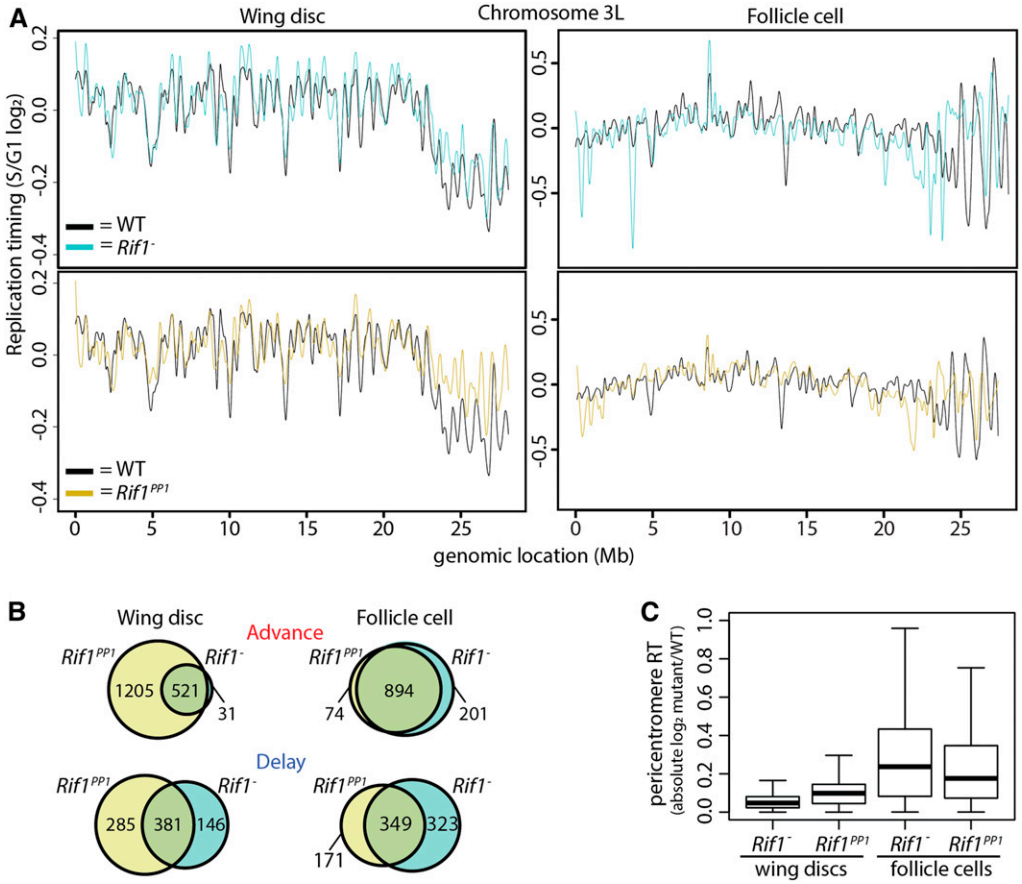

Figure 6 Rif1's PP1 binding motif is essential for Rif1-mediated RT control. (A) LOESS regression line showing average *Rif1*$^{-}$ (cyan), *Rif1*^{PP1} (gold), and wild-type (black) S/G1 (log_2) replication timing values in wing discs (left) and follicle cells (right) across the chromosome 3L scaffold. See Figures S6, S7, S12, and S13 for other chromosomes. (B) Venn diagrams comparing significantly advanced (top) and delayed (bottom) 100-kb windows identified in *Rif1*$^{-}$ (cyan) and *Rif1*^{PP1} (gold) wing discs (left) and follicle cells (right) ($P < 0.01$ and absolute log_2 fold change > 0.1; limma). (C) Box plot of absolute mutant/control log_2 ratio of normalized replication timing values [S/G1 (log_2)] at all pericentromeric regions of the major chromosome scaffolds.

We found that ~30% of the genome had different RT in the two tissue types we examined, and that changes in transcript levels do not account for these changes. Studies in other systems also have failed to establish a direct relationship between changes in RT and changes in transcript levels (MacAlpine *et al.* 2004; Lubelsky *et al.* 2014; Rivera-Mulia *et al.* 2015; Siefert *et al.* 2017; Almeida *et al.* 2018; Armstrong *et al.* 2018). While transcriptional activity has long been correlated with RT, there are clearly mechanisms that control RT independently of transcription. RT is highly correlated with genome topology (Pope *et al.* 2014), and recent work has demonstrated that changes in TAD structure can be uncoupled from changes in gene expression (Ghavi-Helm *et al.* 2019). Therefore, our results are consistent with a model in which lineage-specific changes in genome topology, not transcription, underlie changes to the RT program as cells differentiate. These RT programs can then further be enforced by *trans*-acting factors such as Rif1.

When comparing different tissues, we found a higher degree of overlap between regions of the genome that transition from late to early in the absence of Rif1 than those that transition from early to late. These data imply that Rif1 directly promotes late replication of specific regions of the genome while indirectly affecting regions of the genome that normally replicate early. It is currently unknown, however, how Rif1 is targeted to heterochromatin and other late-replicating regions of the genome to delay RT. Rif1 dynamically associates with heterochromatin from yeasts to humans (Buonomo *et al.* 2009; Seller and O'Farrell 2018). In early *Drosophila* embryos, Rif1 is recruited to heterochromatic regions independently of HP1a, and then displaced from heterochromatin immediately before heterochromatin is replicated late in S phase (Seller and O'Farrell 2018). Chromatin immunoprecipitation of Rif1 followed by sequencing has revealed that in yeast and mouse cells Rif1 targets many other regions of the genome within both late and early-replicating domains (Hayano *et al.* 2012; Foti *et al.* 2016). Our results argue that Rif1 localization to chromatin is likely influenced by cell-type-specific factors.

Our results demonstrate that in metazoans the PP1 interaction motif of Rif1 can contribute to Rif1-mediated RT control. These data suggest that helicase inactivation, or inactivation of another PP1 target near origins of replication, is critical for Rif1-mediated RT control. Multiple models have been proposed to explain how Rif1 controls RT. First, through a direct interaction with PP1, Rif1 is thought to counteract DDK-mediated helicase activation and delay replication of Rif1-associated regions (Davé *et al.* 2014; Hiraga *et al.* 2014; Alver *et al.* 2017). Second, based on 4C experiments with five viewpoints, Rif1 was shown to affect chromatin contacts between different RT domains, suggesting that Rif1 controls RT through nuclear organization (Foti *et al.* 2016). It is unclear

how these different models are related, if at all. Furthermore, while the timing decision point occurs in G1 phase, helicase activation occurs throughout S phase, raising additional mechanistic questions about how Rif1 controls RT. Previous work in budding yeast has shown that DDK can act in G1 phase (Heller *et al.* 2011; Tanaka *et al.* 2011; Zhang *et al.* 2019). Additionally, DDK-dependent helicase activation and Cdc45 recruitment in G1 phase is critical for the specification of certain replication origins. Thus, premature helicase activation in the absence of Rif1 during G1 phase could alter the localization of specific replication domains. While this model could unify the observations describing how Rif1 controls RT, further work is needed to test this possibility.

Our data suggest that different regulatory mechanisms control late RT between wing discs and follicle cells. The approximate threefold increase in the number of windows with advanced RT in *Rif1*^{PP1} wing discs relative to *Rif1*$^{-}$ null wing discs was surprising. These data indicate that the presence of mutant Rif1^{PP1} protein results in a stronger effect than the absence of Rif1. One possibility is that Rif1^{PP1} acts in a dominant negative manner in regions of the genome that normally replicate late during S phase, such as pericentric heterochromatin. Another striking observation was that loss of Rif1 function in wing discs did not substantially advance RT in much of the pericentric heterochromatin. This result suggests that mechanisms in addition to Rif1/PP1-mediated MCM dephosphorylation act within the wing disc to promote late replication of pericentric heterochromatin.

In summary, our study demonstrates that cell lineage is a major driver of RT control within the context of a developing organism. Rif1 fine tunes the RT program established in different tissues, and each of these modes of RT control function independently of transcriptional control, suggesting additional levels of regulation.

Acknowledgments

This work was supported by National Institutes of Health (NIH) grants R01-GM124201 to R.J.D. and NSF-MCB 1818019 to J.T.N. In addition, R.L.A. was supported in part by NIH predoctoral training grant T32-GM007092. We thank the University of North Carolina, Chapel Hill (UNC) Flow Cytometry and High Throughput Sequencing Core Facilities, supported in part by P30 CA016086 Cancer Center core support grant to the UNC Lineberger Comprehensive Cancer Center. FACS results reported in this publication were supported in part by the North Carolina Biotechnology Center institutional support grant 2012-IDG-1006. Flow cytometry experiments were performed in the Vanderbilt Medical Center (VMC) Flow Cytometry Shared Resource. The VMC Flow Cytometry Shared Resource is supported by the Vanderbilt Ingram Cancer Center (P30 CA68485) and the Vanderbilt Digestive Disease Research Center (DK058404). The authors express no conflict of interest.

Author contributions: R.L.A., S.D., R.J.D., and J.T.N. designed the experiments. R.L.A., C.A.H., and S.D. performed the experiments. R.L.A. performed the bioinformatic and statistical analyses. R.L.A., S.D., R.J.D., and J.T.N. analyzed the data. R.L.A., S.D., and J.T.N. wrote the manuscript. R.L.A., S.D., R.J.D., and J.T.N. edited the manuscript.

Literature Cited

Almeida, R., J. M. Fernández-Justel, C. Santa-María, J.-C. Cadoret, L. Cano-Aroca *et al.*, 2018 Chromatin conformation regulates the coordination between DNA replication and transcription. Nat. Commun. 9: 1590. https://doi.org/10.1038/s41467-018-03539-8

Alver, R. C., G. S. Chadha, P. J. Gillespie, and J. J. Blow, 2017 Reversal of DDK-mediated MCM phosphorylation by Rif1–PP1 regulates replication initiation and replisome stability independently of ATR/Chk1. Cell Rep. 18: 2508–2520. https://doi.org/10.1016/j.celrep.2017.02.042

Armstrong, R. L., T. J. R. Penke, B. D. Strahl, A. G. Matera, D. J. McKay *et al.*, 2018 Chromatin conformation and transcriptional activity are permissive regulators of DNA replication initiation in Drosophila. Genome Res. 28: 1688–1700. https://doi.org/10.1101/gr.239913.118

Bell, S. P., and B. Stillman, 1992 ATP-dependent recognition of eukaryotic origins of DNA replication by a multiprotein complex. Nature 357: 128–134. https://doi.org/10.1038/357128a0

Bolstad, B. M., 2016 preprocessCore: A collection of pre-processing functions. R package version 1.36.0. https://github.com/bmbolstad/preprocessCore

Buonomo, S. B. C., Y. Wu, D. Ferguson, and T. de Lange, 2009 Mammalian Rif1 contributes to replication stress survival and homology-directed repair. J. Cell Biol. 187: 385–398. https://doi.org/10.1083/jcb.200902039

Calvi, B. R., M. A. Lilly, and A. C. Spradling, 1998 Cell cycle control of chorion gene amplification. Genes Dev. 12: 734–744. https://doi.org/10.1101/gad.12.5.734

Cayirlioglu, P., W. O. Ward, S. C. Silver Key, and R. J. Duronio, 2003 Transcriptional repressor functions of Drosophila E2F1 and E2F2 cooperate to inhibit genomic DNA synthesis in ovarian follicle cells. Mol. Cell. Biol. 23: 2123–2134. https://doi.org/10.1128/MCB.23.6.2123-2134.2003

Collart, C., G. E. Allen, C. R. Bradshaw, J. C. Smith, and P. Zegerman, 2013 Titration of Four replication factors is essential for the Xenopus laevis midblastula transition. Science 341: 893–896. https://doi.org/10.1126/science.1241530

Cornacchia, D., V. Dileep, J. P. Quivy, R. Foti, F. Tili *et al.*, 2012 Mouse Rif1 is a key regulator of the replication-timing programme in mammalian cells. EMBO J. 31: 3678–3690. https://doi.org/10.1038/emboj.2012.214

Davé, A., C. Cooley, M. Garg, and A. Bianchi, 2014 Protein phosphatase 1 recruitment by Rif1 regulates DNA replication origin firing by counteracting DDK activity. Cell Rep. 7: 53–61. https://doi.org/10.1016/j.celrep.2014.02.019

Donley, N., and M. J. Thayer, 2013 DNA replication timing, genome stability and cancer: late and/or delayed DNA replication timing is associated with increased genomic instability. Semin. Cancer Biol. 23: 80–89. https://doi.org/10.1016/j.semcancer.2013.01.001

Eaton, M. L., J. A. Prinz, H. K. MacAlpine, G. Tretyakov, P. V. Kharchenko *et al.*, 2011 Chromatin signatures of the *Drosophila* replication program. Genome Res. 21: 164–174. https://doi.org/10.1101/gr.116038.110

Edgar, B. A., and T. L. Orr-Weaver, 2001 Endoreplication cell cycles: more for less. Cell 105: 297–306. https://doi.org/10.1016/S0092-8674(01)00334-8

Edgar, B. A., N. Zielke, and C. Gutierrez, 2014 Endocycles: a recurrent evolutionary innovation for post-mitotic cell growth. Nat. Rev. Mol. Cell Biol. 15: 197–210 (erratum: Nat. Rev. Mol. Cell Biol. 15: 294). https://doi.org/10.1038/nrm3756

Foti, R., S. Gnan, D. Cornacchia, V. Dileep, A. Bulut-Karslioglu *et al.*, 2016 Nuclear architecture organized by Rif1 underpins the replication-timing program. Mol. Cell 61: 260–273. https://doi.org/10.1016/j.molcel.2015.12.001

Fox, D. T., and R. J. Duronio, 2013 Endoreplication and polyploidy: insights into development and disease. Development 140: 3–12. https://doi.org/10.1242/dev.080531

Ghavi-Helm, Y., A. Jankowski, S. Meiers, R. R. Viales, J. O. Korbel *et al.*, 2019 Highly rearranged chromosomes reveal uncoupling between genome topology and gene expression. Nat. Genet. 51: 1272–1282. https://doi.org/10.1038/s41588-019-0462-3

Hayano, M., Y. Kanoh, S. Matsumoto, C. Renard-Guillet, K. Shirahige *et al.*, 2012 Rif1 is a global regulator of timing of replication origin firing in fission yeast. Genes Dev. 26: 137–150. https://doi.org/10.1101/gad.178491.111

Heller, R. C., S. Kang, W. M. Lam, S. Chen, C. S. Chan *et al.*, 2011 Eukaryotic origin-dependent DNA replication in vitro reveals sequential action of DDK and S-cdk kinases. Cell 146: 80–91. https://doi.org/10.1016/j.cell.2011.06.012

Hiraga, S.-i., G. M. Alvino, F. Chang, H.-y. Lian, A. Sridhar *et al.*, 2014 Rif1 controls DNA replication by directing Protein Phosphatase 1 to reverse Cdc7-mediated phosphorylation of the MCM complex. Genes Dev. 28: 372–383. https://doi.org/10.1101/gad.231258.113

Hiraga, S. i., T. Ly, J. Garzón, Z. Hořejší, Y. Ohkubo *et al.*, 2017 Human RIF1 and protein phosphatase 1 stimulate DNA replication origin licensing but suppress origin activation. EMBO Rep. 18: 403–419. https://doi.org/10.15252/embr.201641983

Hiratani, I., T. Ryba, M. Itoh, T. Yokochi, M. Schwaiger *et al.*, 2008 Global reorganization of replication domains during embryonic stem cell differentiation. PLoS Biol. 6: e245. https://doi.org/10.1371/journal.pbio.0060245

Hiratani, I., T. Ryba, M. Itoh, J. Rathjen, M. Kulik *et al.*, 2010 Genome-wide dynamics of replication timing revealed by in vitro models of mouse embryogenesis. Genome Res. 20: 155–169. https://doi.org/10.1101/gr.099796.109

Hua, B. L., G. W. Bell, H. Kashevsky, J. R. Von Stetina, and T. L. Orr-Weaver, 2018 Dynamic changes in ORC localization and replication fork progression during tissue differentiation. BMC Genomics 19: 623. https://doi.org/10.1186/s12864-018-4992-3

Karolchik, D., A. S. Hinrichs, T. S. Furey, K. M. Roskin, C. W. Sugnet *et al.*, 2004 The UCSC Table Browser data retrieval tool. Nucleic Acids Res. 32: D493–D496. https://doi.org/10.1093/nar/gkh103

Kharchenko, P. V., A. A. Aleksyenko, Y. B. Schwartz, A. Minoda, N. C. Riddle *et al.*, 2011 Comprehensive analysis of the chromatin landscape in Drosophila melanogaster. Nature 471: 480–485. https://doi.org/10.1038/nature09725

Kim, J. C., J. Nordman, F. Xie, H. Kashevsky, T. Eng *et al.*, 2011 Integrative analysis of gene amplification in Drosophila follicle cells: parameters of origin activation and repression. Genes Dev. 25: 1384–1398. https://doi.org/10.1101/gad.2043111

Koren, A., P. Polak, J. Nemesh, J. J. Michaelson, J. Sebat *et al.*, 2012 Differential relationship of DNA replication timing to different Forms of human mutation and variation. Am. J. Hum. Genet. 91: 1033–1040. https://doi.org/10.1016/j.ajhg.2012.10.018

Langmead, B., C. Trapnell, M. Pop, and S. L. Salzberg, 2009 Ultrafast and memory-efficient alignment of short DNA sequences to the human genome. Genome Biol. 10: R25. https://doi.org/10.1186/gb-2009-10-3-r25

Li, H., B. Handsaker, A. Wysoker, T. Fennell, J. Ruan *et al.*, 2009 The sequence alignment/map format and SAMtools. Bioinformatics 25: 2078–2079. https://doi.org/10.1093/bioinformatics/btp352

Lilly, M. A., and A. C. Spradling, 1996 The Drosophila endocycle is controlled by Cyclin E and lacks a checkpoint ensuring S-phase completion. Genes Dev. 10: 2514–2526. https://doi.org/10.1101/gad.10.19.2514

Liu, J., K. McConnell, M. Dixon, and B. R. Calvi, 2012 Analysis of model replication origins in *Drosophila* reveals new aspects of the chromatin landscape and its relationship to origin activity and the prereplicative complex. Mol. Biol. Cell 23: 200–212. https://doi.org/10.1091/mbc.e11-05-0409

Lubelsky, Y., J. A. Prinz, L. DeNapoli, Y. Li, J. A. Belsky *et al.*, 2014 DNA replication and transcription programs respond to the same chromatin cues. Genome Res. 24: 1102–1114. https://doi.org/10.1101/gr.160010.113

MacAlpine, D. M., H. K. Rodriguez, and S. P. Bell, 2004 Coordination of replication and transcription along a *Drosophila* chromosome. Genes Dev. 18: 3094–3105. https://doi.org/10.1101/gad.1246404

MacAlpine, H. K., R. Gordân, S. K. Powell, A. J. Hartemink, and D. M. MacAlpine, 2010 Drosophila ORC localizes to open chromatin and marks sites of cohesin complex loading. Genome Res. 20: 201–211. https://doi.org/10.1101/gr.097873.109

Mantiero, D., A. Mackenzie, A. Donaldson, and P. Zegerman, 2011 Limiting replication initiation factors execute the temporal programme of origin firing in budding yeast. EMBO J. 30: 4805–4814. https://doi.org/10.1038/emboj.2011.404

Maqbool, S. B., S. Mehrotra, A. Kolpakas, C. Durden, B. Zhang *et al.*, 2010 Dampened activity of E2F1-DP and Myb-MuvB transcription factors in Drosophila endocycling cells. J. Cell Sci. 123: 4095–4106. https://doi.org/10.1242/jcs.064519

Mattarocci, S., M. Shyian, L. Lemmens, P. Damay, D. M. Altintas *et al.*, 2014 Rif1 controls DNA replication timing in yeast through the PP1 phosphatase Glc7. Cell Rep. 7: 62–69. https://doi.org/10.1016/j.celrep.2014.03.010

McCarthy, D. J., Y. Chen, and G. K. Smyth, 2012 Differential expression analysis of multifactor RNA-Seq experiments with respect to biological variation. Nucleic Acids Res. 40: 4288–4297. https://doi.org/10.1093/nar/gks042

Miotto, B., Z. Ji, and K. Struhl, 2016 Selectivity of ORC binding sites and the relation to replication timing, fragile sites, and deletions in cancers. Proc. Natl. Acad. Sci. USA 113: E4810–E4819. https://doi.org/10.1073/pnas.1609060113

Munden, A., Z. Rong, A. Sun, R. Gangula, S. Mallal *et al.*, 2018 Rif1 inhibits replication fork progression and controls DNA copy number in Drosophila. eLife 7: e39140. https://doi.org/10.7554/eLife.39140

Newville, M., T. Stensitzki, D. B. Allen, and A. Ingargiola, 2014- *LMFIT: Non-Linear Least-Square Minimization and Curve-Fitting for Python*, Zenodo. https://doi.org/10.5281/zenodo.11813

Peace, J. M., A. Ter-Zakarian, and O. M. Aparicio, 2014 Rif1 regulates initiation timing of late replication origins throughout the *S. cerevisiae* genome. PLoS One 9: e98501. https://doi.org/10.1371/journal.pone.0098501

Pope, B. D., T. Ryba, V. Dileep, F. Yue, W. Wu *et al.*, 2014 Topologically associating domains are stable units of replication-timing regulation. Nature 515: 402–405. https://doi.org/10.1038/nature13986

Quinlan, A. R., and I. M. Hall, 2010 BEDTools: a flexible suite of utilities for comparing genomic features. Bioinformatics 26: 841–842. https://doi.org/10.1093/bioinformatics/btq033

Rivera-Mulia, J. C., and D. M. Gilbert, 2016 Replication timing and transcriptional control: beyond cause and effect — part III.

Curr. Opin. Cell Biol. 40: 168–178. https://doi.org/10.1016/j.ceb.2016.03.022

Rivera-Mulia, J. C., Q. Buckley, T. Sasaki, J. Zimmerman, R. A. Didier *et al.*, 2015 Dynamic changes in replication timing and gene expression during lineage specification of human pluripotent stem cells. Genome Res. 25: 1091–1103. https://doi.org/10.1101/gr.187989.114

Robinson, M. D., D. J. McCarthy, and G. K. Smyth, 2010 edgeR: a Bioconductor package for differential expression analysis of digital gene expression data. Bioinformatics 26: 139–140. https://doi.org/10.1093/bioinformatics/btp616

Rotelli, M. D., R. A. Policastro, A. M. Bolling, A. W. Killion, A. J. Weinberg *et al.*, 2019 A Cyclin A-Myb-MuvB-Aurora B network regulates the choice between mitotic cycles and polyploid endoreplication cycles. PLoS Genet. 15: e1008253. https://doi.org/10.1371/journal.pgen.1008253

Ryba, T., I. Hiratani, J. Lu, M. Itoh, M. Kulik *et al.*, 2010 Evolutionarily conserved replication timing profiles predict long-range chromatin interactions and distinguish closely related cell types. Genome Res. 20: 761–770. https://doi.org/10.1101/gr.099655.109

Schwaiger, M., M. B. Stadler, O. Bell, H. Kohler, E. J. Oakeley *et al.*, 2009 Chromatin state marks cell-type- and gender-specific replication of the Drosophila genome. Genes Dev. 23: 589–601. https://doi.org/10.1101/gad.511809

Seller, C. A., and P. H. O'Farrell, 2018 Rif1 prolongs the embryonic S phase at the Drosophila mid-blastula transition. PLoS Biol. 16: e2005687. https://doi.org/10.1371/journal.pbio.2005687

Sher, N., G. W. Bell, S. Li, J. T. Nordman, T. Eng *et al.*, 2012 Developmental control of gene copy number by repression of replication initiation and fork progression. Genome Res. 22: 64–75. https://doi.org/10.1101/gr.126003.111

Siefert, J. C., C. Georgescu, J. D. Wren, A. Koren, and C. L. Sansam, 2017 DNA replication timing during development anticipates transcriptional programs and parallels enhancer activation. Genome Res. 27: 1406–1416. https://doi.org/10.1101/gr.218602.116

Sreesankar, E., V. Bharathi, R. K. Mishra, and K. Mishra, 2015 Drosophila Rif1 is an essential gene and controls late developmental events by direct interaction with PP1–87B. Sci. Rep. 5: 10679 [corrigenda: Sci. Rep. 6: 17126 (2016)]. https://doi.org/10.1038/srep17126

Stamatoyannopoulos, J. A., I. Adzhubei, R. E. Thurman, G. V. Kryukov, S. M. Mirkin *et al.*, 2009 Human mutation rate associated with DNA replication timing. Nat. Genet. 41: 393–395. https://doi.org/10.1038/ng.363

Sukackaite, R., D. Cornacchia, M. R. Jensen, P. J. Mas, M. Blackledge *et al.*, 2017 Mouse Rif1 is a regulatory subunit of protein phosphatase 1 (PP1). Sci. Rep. 7: 2119. https://doi.org/10.1038/s41598-017-01910-1

Tanaka, S., R. Nakato, Y. Katou, K. Shirahige, and H. Araki, 2011 Origin association of Sld3, Sld7, and Cdc45 proteins is a key step for determination of origin-firing timing. Curr. Biol. 21: 2055–2063. https://doi.org/10.1016/j.cub.2011.11.038

Trapnell, C., A. Roberts, L. Goff, G. Pertea, D. Kim *et al.*, 2012 Differential gene and transcript expression analysis of RNA-seq experiments with TopHat and Cufflinks. Nat. Protoc. 7: 562–578 [corrigenda: Nat. Protoc. 9: 2513 (2014)]. https://doi.org/10.1038/nprot.2012.016

Yamazaki, S., A. Ishii, Y. Kanoh, M. Oda, Y. Nishito *et al.*, 2012 Rif1 regulates the replication timing domains on the human genome. EMBO J. 31: 3667–3677. https://doi.org/10.1038/emboj.2012.180

Zhang, H., M. V. Petrie, Y. He, J. M. Peace, I. E. Chiolo *et al.*, 2019 Dynamic relocalization of replication origins by Fkh1 requires execution of DDK function and Cdc45 loading at origins. eLife 8: e45512. https://doi.org/10.7554/eLife.45512

Communicating editor: B. Calvi